IEEE Access
Multidisciplinary | Rapid Review | Open Access Journal

Date of publication xxxx 00, 0000, date of current version February 2, 2021.

Digital Object Identifier 10.1109/ACCESS.2017.DOI

A Stochastic Geometry Approach to EMF Exposure Modeling

QUENTIN GONTIER[1], LUCA PETRILLO[2], FRANÇOIS ROTTENBERG[3], (MEMBER, IEEE), FRANÇOIS HORLIN[1], (MEMBER, IEEE) , JOE WIART[4], (SENIOR MEMBER, IEEE), CLAUDE OESTGES[5], (FELLOW, IEEE), AND PHILIPPE DE DONCKER[1], (MEMBER, IEEE)

[1]Wireless Communications Group, Université libre de Bruxelles, Belgium (e-mail: firstname.lastname@ulb.ac.be)
[2]Brussels Environment, Belgium (e-mail: lpetrillo@environnement.brussels)
[4]ESAT-DRAMCO, Ghent Technology Campus, KU Leuven, 9000 Ghent, Belgium (e-mail: francois.rottenberg@kuleuven.be)
[4]LTCI, Telecom Paris, Chaire C2M, Institut Polytechnique de Paris, Palaiseau 91120, France (e-mail: joe.wiart@telecom-paris.fr)
[5]ICTEAM Institute, Université catholique de Louvain, B-1348 Louvain-la-Neuve, Belgium (e-mail: claude.oestges@uclouvain.be).

Corresponding author: Quentin Gontier (e-mail: quentin.gontier@ulb.be).

This work was supported in part by the FNRS under MUSE-WINET EOS grant and Innoviris under STOEMP-EMF grant.

ABSTRACT Downlink exposure to electromagnetic fields due to cellular base stations in urban environments is studied using the stochastic geometry framework. A two-dimensional Poisson point process is assumed for the base station distribution. Mathematical expressions of statistics of exposure are derived from a simple propagation model taking into account the height of the base stations. The error on exposure made by taking a limited number of base stations, instead of the whole set, is quantified. The relative impact of the model parameters on the statistics of exposure is highlighted. The method is then applied and the model parameters are calibrated using experimental data obtained by drive-tests in two Brussels municipalities, in Belgium, for the 2100 MHz and 2600 MHz frequency bands. It is shown that the proposed model fits experimental values, paving the way to a new methodology to assess general public exposure to electromagnetic fields, for any frequency band. An insight is given on how to apply the methodology to a real case without access to experimental data.

INDEX TERMS cellular networks, exposure, Poisson point process, stochastic geometry

I. INTRODUCTION

Electromagnetic field (EMF) exposure due to cellular networks is classically evaluated empirically either through in-situ measurements [1], drive-tests [2], [3] or sensor networks [4]. Numerically, this evaluation, either by using ray-launching softwares [5], ray-tracing softwares [6] or other simulation methods based on propagation models [7]–[9], is however difficult to obtain deterministically in a reasonable time. It is also subject to many uncertainties (due to the number of base stations in operation, the environment geometry, the presence of people and vehicles causing shadowing...). A deterministic computation of EMF exposure at every point of the area under study is not always required. Instead, statistical values are often looked for, for instance to estimate the probability of exceeding some exposure thresholds, or to estimate the mean level of exposure. Numerous studies developed statistical models for exposure assessment as in [10] for 5G radio base stations using massive MIMO or in [11] for a WiFi source in an apartment, based on the Kriging method. There is however a lack of models able to quickly, accurately and with a limited number of parameters, determine exposure statistics in a real environment of a scale larger than a few thousand square meters, without a deterministic knowledge of the environment geometry. This paper aims to lay foundations of an entirely new stochastic approach to assess exposure to electromagnetic fields due to cellular networks, using stochastic geometry (SG) and a simple parametric propagation model.

Using SG in wireless communications is not a new concept [12]. It has been applied in many fields, ranging from automotive radar [13], to localization [14], including probability of coverage and spectral efficiency [15], cumulated interference power [16] and outage probability [17] but to our knowledge, only one recent paper exploits it for exposure assessment [18]. The latter is a first attempt to model exposure in millimeter wave bands, based on empirical propagation models. But neither in-depth theoretical study, nor experimental validation of the proposed models are included.

This article has been accepted for publication in a future issue of this journal, but has not been fully edited. Content may change prior to final publication. Citation information: DOI 10.1109/ACCESS.2021.3091804, IEEE Access

EMF exposure is usually characterized in terms of incident power density S (W/m^2) [19], [20]. Power density may then be translated into root-mean-square electric field strength (V/m), as used in exposure standards:

$$E = \sqrt{Z_0\, S} \tag{1}$$

where $Z_0 = \sqrt{\mu_0/\epsilon_0} = 120\pi \approx 377\Omega$ is the impedance of free-space.

In the first part of this paper, mathematical expressions are derived to evaluate the statistics and cumulative distribution function (CDF) of the power density emitted by a random pattern of cellular base stations (BSs). The error made by including only the few BSs closest to the calculation point is evaluated. In the second part, we calibrate and validate the model using experimental data obtained in two municipalities of the Brussels-Capital Region, in Belgium, in the 2100 MHz and the 2600 MHz frequency bands.

II. STOCHASTIC GEOMETRY MODEL OF EXPOSURE

A. EXPOSURE MODEL

In the SG approach, the BS spatial distribution for a given cellular frequency band is considered as a random point pattern with constant density λ in a given 2D region $\mathcal{W}$, referred to as the window. According to [21], considering together the BSs of all network providers as required for exposure assessment, BS spatial distributions for any cellular frequency band in European cities are well modeled using homogeneous 2D-Poisson Point Processes $\Phi \in \mathbb{R}^2$ (PPP): for any $\mathcal{W}$, the number of points falling in $\mathcal{W}$ has a Poisson distribution with mean $\lambda \cdot \tau_2(\mathcal{W})$,where $\tau_2(\mathcal{W})$ is the area of $\mathcal{W}$. It implies that measures do not depend on the location in space where the computation is performed. More details about stochastic geometry and its applications to cellular networks can be found in Kingman's book [22] or the paper by Andrews et al. [17].

For any BS of the PPP, the incident power density S can be deduced from a path loss model

$$S(r) = \frac{A}{\left(r^2 + h^2\right)^{\alpha/2}}, \tag{2}$$

where $S(r)$ is the power density due to the BS located at a horizontal distance r, h the height of the BS, α the path loss exponent (typically ranging from 2 to 5) and A a multiplicative random variable modeling channel fading and the effective isotropic radiated power (EIRP) of the BS. A can be written $A = p \cdot B$ with $p = \frac{\text{EIRP}}{4\pi}$ and B is any random variable modeling fading. In the following, the expected value of A, $\mathbb{E}[A]$, will be noted $\overline{A}$. It is worth noting that, in our approach, the BS network is homogenized in the sense that BSs share common features in terms of height and EIRP.

For all BSs of all network providers present in the PPP, the power densities can be summed up, assuming that all signals are uncorrelated, to get S_{WN}, the total EMF power density and hence the total exposure for the whole network of BSs (WN) in a determined frequency band

$$S_{WN} = \sum_{i|BS_i \in \Phi} S(r_i) = \sum_{i|BS_i \in \Phi} \frac{A}{\left(h^2 + r_i^2\right)^{\alpha/2}}. \tag{3}$$

B. EXPOSURE DUE TO THE n^{th} NEAREST BASE STATION

We start by studying separately the contribution of each BS of the PPP. Let $S_n = S_n(r)$ be the power density due to the n^{th} nearest BS to the calculation point. The probability density function (PDF) of the distance r_n to the n^{th} nearest BS is given by the Erlang distribution of order n [23]

$$f(r_n) = 2\frac{(\lambda\pi)^n}{(n-1)!}\, r_n^{2n-1}\, \mathrm{e}^{-\lambda\pi r_n^2}. \tag{4}$$

The expected power density due to the n^{th} nearest BS is given in the following theorem.

Theorem 1. *The expected power density due to the n^{th} nearest BS is*

$$\mathbb{E}[S_n] = \overline{A}\,(\lambda\pi)^{\alpha/2}\, \mathrm{e}^{\lambda\pi h^2}\, \sigma^n_{\{-\alpha/2\}},$$
$$\sigma^i_{\{x\}} = \sum_{l=0}^{i-1} \frac{\left(-\lambda\pi h^2\right)^{i-l-1}}{l!\,(i-l-1)!}\, \tilde{\Gamma}_{1+l+x}.$$

Proof. From the independence between A and the distance r_n and from the use of the Erlang distribution (4) of order n, it follows that

$$\mathbb{E}[S_n] = \overline{A}\,\frac{2\,(\lambda\pi)^n}{(n-1)!} \int_0^\infty \frac{1}{\left(r^2+h^2\right)^{\alpha/2}}\, r^{2n-1}\, \mathrm{e}^{-\lambda\pi r^2}\, \mathrm{d}r.$$

Using the change of variable $r^2 \to \frac{t}{\lambda\pi} - h^2$ and the Binomial theorem, this expression becomes

$$\mathbb{E}[S_n] = \overline{A}\,\frac{(\lambda\pi)^n\,(\lambda\pi)^{\alpha/2-1}}{(n-1)!}\, \mathrm{e}^{\lambda\pi h^2} \int_{\lambda\pi h^2}^\infty t^{-\alpha/2} \times \mathrm{e}^{-t} \sum_{l=0}^{n-1} \binom{n-1}{l} \left(\frac{t}{\lambda\pi}\right)^l \left(-h^2\right)^{n-1-l} \mathrm{d}t.$$

Theorem 1 is then obtained by using the upper incomplete Gamma function $\Gamma(z,t)$ defined as

$$\Gamma(z,t) = \int_t^\infty u^{z-1}\, \mathrm{e}^{-u}\, \mathrm{d}u, \qquad \Re(z) > 0. \tag{5}$$

□

$\tilde{\Gamma}_i$ is used as a simplified notation for $\Gamma\left(i, \lambda\pi h^2\right)$. When $\alpha > 2$, the incomplete Gamma function is not properly defined since the first argument of the incomplete Gamma function is sometimes negative. In this case, the Gauss

This article has been accepted for publication in a future issue of this journal, but has not been fully edited. Content may change prior to final publication. Citation information: DOI 10.1109/ACCESS.2021.3091804, IEEE Access

continued fraction can nonetheless be used for numerical calculations [24]

$$\Gamma(z,t) = \cfrac{t^z \mathrm{e}^{-t}}{t + \cfrac{1-z}{1 + \cfrac{1}{t + \cfrac{2-z}{1 + \cfrac{2}{t + \cfrac{3-z}{1 + \ddots}}}}}} \tag{6}$$

Simplifications can be made when considering the nearest BS. They lead to the next corollary.

Corollary 1. *The mean value of the power density due to the nearest BS is*

$$\mathbb{E}\left[S_1\right] = (\lambda\pi)^{\alpha/2}\, \overline{A}\, \mathrm{e}^{\lambda\pi h^2}\, \Gamma\left(1 - \frac{\alpha}{2}, \lambda\pi h^2\right).$$

Using Corollary 1, Theorem 1 can also be written as

$$\mathbb{E}\left[S_n\right] = \mathbb{E}\left[S_1\right] \cdot \Xi_n^{[1]} \tag{7}$$

where

$$\Xi_n^{[1]} = \frac{\sigma^n_{\{-\alpha/2\}}}{\tilde{\Gamma}_{1-\alpha/2}} = \sum_{l=1}^{n} \frac{\left(-\lambda\pi h^2\right)^{n-l}}{(l-1)!\,(n-l)!} \frac{\tilde{\Gamma}_{l-\alpha/2}}{\tilde{\Gamma}_{1-\alpha/2}}, \tag{8}$$

using the change of index $l+1 \to l$. Fig. 1 shows the ratio (8) as a function of n. As can be seen from this figure, for the sets of parameters that will be identified in section III, the nearest BS provides the main contribution to exposure but the second BS is also important since the ratio $\mathbb{E}\left[S_2\right]/\mathbb{E}\left[S_1\right]$ is around 15%. From the fourth nearest BS, the contribution is lower than 5% for both sets of parameters. Note that $\Xi_n^{[1]}$ is dependent on the values of the model parameters. Nonetheless, from this figure, we see that $\Xi_n^{[1]}$ has a nearly logarithmic decay. A physical intuition can be given by observing the following proposition.

Proposition 1. *The ratio between the expected values of the inverse of the distance to the n^{th} nearest BS, $1/r_n$, and the inverse of the distance to the nearest BS, $1/r_1$, asymptotically has a logarithmic decrease.*

Proof. The expected value of the inverse of the distance to the n^{th} nearest BS, $1/r_n$, is, by using (4)

$$\mathbb{E}\left[\frac{1}{r_n}\right] = \frac{\Gamma\left(n - 1/2\right)}{\sqrt{\lambda\,\pi}\,(n-1)!}.$$

The logarithm of the ratio between $\mathbb{E}\left[1/r_n\right]$ and $\mathbb{E}\left[1/r_1\right]$ is then

$$\log \frac{\mathbb{E}\left[1/r_n\right]}{\mathbb{E}\left[1/r_1\right]} = \log \frac{\Gamma\left(n - \frac{1}{2}\right)}{(n-1)!\,\Gamma\left(\frac{1}{2}\right)} = \log \frac{(2\,(n-1))!}{2^{2n-2}\,\left[(n-1)!\right]^2}$$

Using Stirling's approximation, the ratio becomes

$$\log \frac{\mathbb{E}\left[1/r_n\right]}{\mathbb{E}\left[1/r_1\right]} = \log \frac{1}{\sqrt{\pi\,(n-1)}} + \log\left(1+\epsilon_1\right) - 2\log\left(1+\epsilon_2\right)$$

with

$$\epsilon_1 = O\left(\frac{1}{2(n-1)}\right), \quad \epsilon_2 = O\left(\frac{1}{n-1}\right).$$

This can be further simplified to give

$$\log \frac{\mathbb{E}\left[1/r_n\right]}{\mathbb{E}\left[1/r_1\right]} = \log \frac{1}{\sqrt{\pi\,(n-1)}} + \epsilon, \qquad \epsilon = O\left(\frac{1}{n}\right).$$

Taking the limit to the infinity leads to

$$\lim_{n\to\infty} \log \frac{\mathbb{E}\left[1/r_n\right]}{\mathbb{E}\left[1/r_1\right]} = -\frac{1}{2}\log n - \frac{1}{2}\log \pi.$$

□

Proposition 1 shows a logarithmic decrease. When $r_n >> h$, which is usually quickly the case, S_n can be approximated by A/r_n^{α}, therefore it is not surprising that $\Xi_n^{[1]}$ has a logarithmic decrease.

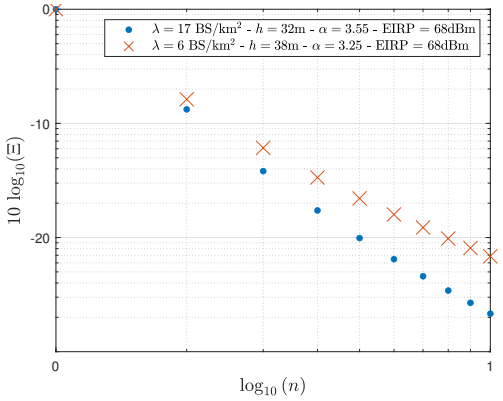

FIGURE 1. Ratio between the mean value of the power density coming from the n^{th} nearest BS and the mean value of the power density coming from the nearest BS as a function of n.

We also give here as Theorem 2 and Corollary 3 the k^{th} moment and the variance of the power density received from the n^{th} nearest BS.

Theorem 2. *The moment of order k of the power density received from the n^{th} nearest BS is*

$$\mathbb{E}\left[S_n^k\right] = \overline{A^k}\,(\lambda\pi)^{\frac{k\alpha}{2}}\,\mathrm{e}^{\lambda\pi h^2}\,\sigma^n_{\{-k\alpha/2\}}.$$

Proof. The proof is obtained by a development similar to the proof of Theorem 1. □

Theorem 2 enables to compute any moment of S_n. Again, this equation can make $\mathbb{E}\left[S_1^k\right]$ appear, generalizing $\Xi_n^{[k]}$ for the order k.

$$\mathbb{E}\left[S_n^k\right] = \mathbb{E}\left[S_1^k\right] \cdot \Xi_n^{[k]}, \tag{9}$$

$$\Xi_n^{[k]} = \frac{\sigma^n_{\{-k\alpha/2\}}}{\tilde{\Gamma}_{1-k\alpha/2}} = \sum_{l=1}^{n} \frac{\left(-\lambda\pi h^2\right)^{n-l}}{(l-1)!\,(n-l)!} \frac{\tilde{\Gamma}_{l-k\alpha/2}}{\tilde{\Gamma}_{1-k\alpha/2}}. \tag{10}$$

Theorem 3. *The variance of the power density received from the n^{th} nearest BS is*

$$\mathbb{V}\left[S_n\right] = (\lambda\pi)^{\alpha}\,\mathrm{e}^{\lambda\pi h^2}\left[\overline{A^2}\,\sigma^n_{\{-\alpha\}} - \mathrm{e}^{\lambda\pi h^2}\,\overline{A}^2\left(\sigma^n_{\{-\frac{\alpha}{2}\}}\right)^2\right].$$

This article has been accepted for publication in a future issue of this journal, but has not been fully edited. Content may change prior to final publication. Citation information: DOI 10.1109/ACCESS.2021.3091804, IEEE Access

Proof. The proof is immediate since $\mathbb{V}\left[S_n\right] = \mathbb{E}\left[S_n^2\right] - \left(\mathbb{E}\left[S_n\right]\right)^2$. □

C. EXPOSURE DUE TO THE n NEAREST BASE STATIONS

The mean value of the cumulated power density due to the n nearest BSs, $S_{[n]}$ is given by Theorem 4. The k^{th}-order moment of $S_{[n]}$ is given by Theorem 5.

Theorem 4. *The mean value of the cumulated power density due to the n nearest BSs, $S_{[n]}$ is*

$$\mathbb{E}\left[S_{[n]}\right] = \mathbb{E}\left[\sum_{i=1}^{n} S_i\right] = \overline{A}\left(\lambda\pi\right)^{\alpha/2} \mathrm{e}^{\lambda\pi h^2} \sum_{i=1}^{n} \sigma^i_{\{-\frac{\alpha}{2}\}}.$$

Proof. This theorem directly follows from Theorem 1 and the assumption of uncorrelated BSs. □

The relative error made by truncating the network to the n nearest BSs is shown in Fig. 2. By taking only the closest BS, as often done in exposure studies, an error of around 10% is committed for the sets of parameters calibrated in section III. The error made by truncating the sum of power densities to the first neighbors is dependent on α. The lower α, the higher the relative error hence the number of neighboring BSs to take into account. The whole-network reference $\mathbb{E}\left[S_{WN}\right]$ will be derived in the following section.

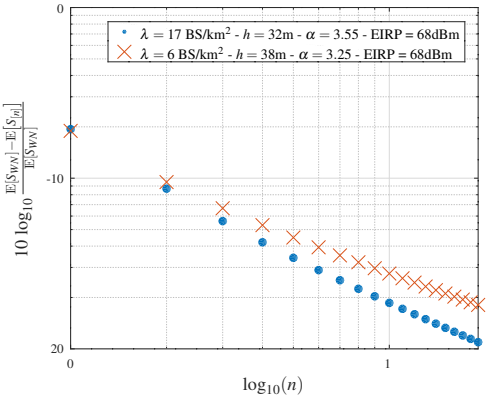

FIGURE 2. Relative error between $\mathbb{E}\left[S_{[n]}\right]$ (4) and $\mathbb{E}\left[S_{WN}\right]$ (6). $\lambda = 6\,\mathrm{BS/km^2}$, $\alpha = 3.25$, $h = 38\,\mathrm{m}$, EIRP = 67.96 dBm.

Theorem 5. *The moment of order k of the cumulated power density due to the n nearest BSs is*

$$\mathbb{E}\left[S^k_{[n]}\right] = \overline{A^k}\left(\lambda\pi\right)^{k\alpha/2} \mathrm{e}^{\lambda\pi h^2} \sum_{|\vec{k}|=k} \binom{k}{\vec{k}} \sum_{p=1}^{n-1} (-1)^{p-1} \times \left(\prod_{j=p+1}^{n-1} \frac{1}{\tau^{(j)}_{(p+1)}}\right) \left(\prod_{l=1}^{p} \frac{1}{\tau^{(p)}_{(l)}}\right) \left[\tilde{\Gamma}_{\tau^{(n)}_{(1)}} - \left(\lambda\pi h^2\right)^{\tau^{(p)}_{(1)}} \tilde{\Gamma}_{\tau^{(n)}_{(p+1)}}\right]$$

where we use the notations

$$\tau_i = 1 - k_i \frac{\alpha}{2}, \qquad \tau^{(b)}_{(a)} = \begin{cases} \sum_{i=a}^{b} \tau_i & \text{if } a \leq b, \\ \tau^{(b)}_{(a)} = 0 & \text{if } a > b. \end{cases}$$

Proof. The proof is given in Appendix A. □

Note that the case $k = 1$ corresponds to Theorem 4. Again, the variance of the distribution can be deduced from Theorem 5.

D. WHOLE NETWORK

Well-known mathematical results of signal-plus-interference-to-noise ratio and power coverage studies [25]–[27] can be adapted to study exposure. The expected value of the power density (3) is given in the following theorem.

Theorem 6. *The expected value of the total power density S_{WN}, distributed according to a PPP $\Phi \in \mathbb{R}^2$, for the propagation model* (3) *with a path loss coefficient $\alpha > 2$, is*

$$\mathbb{E}\left[S_{WN}\right] = \frac{2\pi\lambda\,\overline{A}}{\alpha - 2} \frac{1}{h^{\alpha-2}}.$$

Proof. The calculation is obtained by applying Campbell's formula [22]

$$\mathbb{E}\left[S_{WN}\right] = \lambda\,\overline{A} \int_0^{2\pi} \mathrm{d}\theta \int_0^{\infty} \frac{1}{\left(r^2 + h^2\right)^{\alpha/2}} r\,\mathrm{d}r.$$

□

Theorem 6 clearly shows the relative impact of the BS density, the path loss exponent and the BS height on the mean exposure. Similarly, the variance of the distribution is given as Theorem 7.

Theorem 7. *The variance of the total power density S_{WN}, distributed according to a PPP $\Phi \in \mathbb{R}^2$, for the propagation model* (3) *with a path loss coefficient $\alpha > 2$, is*

$$\mathbb{V}\left[S_{WN}\right] = \frac{2\pi\lambda\,\overline{A^2}}{2\alpha - 2} \frac{1}{h^{2\alpha-2}}$$

with $\overline{A^2} = \mathbb{E}_A\left[A^2\right]$. Theorems 6 and 7 are valid no matter the fading distribution chosen for A.

To obtain the cumulative distribution function of (3), the two-sided Laplace transform of the distribution, $\mathcal{L}_{S_{WN}}$, is needed. The Laplace transform of the distribution of the power density due to a limited number of BSs can be obtained from a power series of the moments of the distribution, given by Theorem 5, but no closed-form expression could be found. The Laplace transform of S_{WN} is given by the following lemma.

Lemma 1. *The Laplace transform of the total power density S_{WN} is given by*

$$\mathcal{L}_{S_{WN}}(s) = \exp\left(\frac{2\pi\lambda}{\alpha} \int_{h^\alpha}^{\infty} \left(\mathbb{E}_A\left[\exp\left(-s\frac{A}{x}\right)\right] - 1\right) x^{\frac{2}{\alpha}-1} \mathrm{d}x\right).$$

Proof. This can be calculated similarly to what is done in [28], chapter 1. The definition of the Laplace transform leads to

$$\mathcal{L}_{S_{WN}}(s) = \mathbb{E}\left[\mathrm{e}^{-s\,S_{WN}}\right] = \mathbb{E}_{\Phi,A}\left[\exp\left(-s\sum_{i\in\Phi} \frac{A}{\left(r_i^2 + h^2\right)^{\alpha/2}}\right)\right].$$

This article has been accepted for publication in a future issue of this journal, but has not been fully edited. Content may change prior to final publication. Citation information: DOI 10.1109/ACCESS.2021.3091804, IEEE Access

Using the probability generating functional [29], this leads to

$$\mathcal{L}_{S_{WN}}(s) = \exp\left(2\pi\lambda \int_0^\infty \mathbb{E}_A\left[\exp\left(\frac{-s\,A}{\left(r^2+h^2\right)^{\alpha/2}}\right)-1\right] r\,\mathrm{d}r\right).$$

Finally, with the change of variable $\left(r^2+h^2\right)^{\alpha/2} \to x$, this expression becomes

$$\mathcal{L}_{S_{WN}}(s) = \exp\left(\frac{2\pi\lambda}{\alpha} \int_{h^\alpha}^\infty \mathbb{E}_A\left[\exp\left(-s\,\frac{A}{x}\right)-1\right] x^{2/\alpha-1}\mathrm{d}x\right).$$

□

$\mathbb{E}_A\left[\exp\left(-s\,\frac{A}{x}\right)\right]$ corresponds to the Laplace transform of A/x. The Laplace transform $\mathcal{L}_{S_{WN}}$ can therefore be calculated if the distribution of A is known. Theorems 8 and 9 respectively give the Laplace transform for A deterministic and A following an exponential distribution.

Theorem 8. *The Laplace transform of the total power density for the no-fading case is*

$$\mathcal{L}^{determ.}_{S_{WN}}(s) = \exp\left(\pi\lambda\,h^2\left[1 - {}_1F_1\left(-\frac{2}{\alpha}; 1-\frac{2}{\alpha}; \frac{-s\,A}{h^\alpha}\right)\right]\right).$$

Proof. Under the no-fading hypothesis, i.e. for A deterministic,

$$\mathbb{E}_A\left[\exp\left(-s\,\frac{A}{x}\right)\right] = \exp\left(-s\,\frac{A}{x}\right).$$

Theorem 8 is then obtained using the relationship [30] in combination with Lemma 1

$$\int_a^\infty \left(\exp\left(\frac{b}{z}\right)-1\right) z^{v-1}\mathrm{d}z = \frac{1}{v}\,a^v\,\left[1 - {}_1F_1\left(-v; 1-v; {}^b/_a\right)\right]$$

where ${}_1F_1(a;b;z)$ is the Kummer confluent hypergeometric function. □

Proposition 2 corresponds to an excellent approximation of the expression of Theorem 8 given by [27], which can be used for numerical calculations.

Proposition 2. *An approximation of the Laplace transform of the total power density for the no-fading case is*

$$\mathcal{L}^{determ.}_{S_{WN}}(s) \approx \begin{cases} \mathrm{e}^{\pi\lambda\,h^2\,\sum_{j=1}^{\infty}\frac{2\,(-sA)^j}{h^{\alpha\,j}\,j!\,(j\,\alpha-2)}}, & \left|\frac{s\,A}{h^\alpha}\right| \le c, \\ \mathrm{e}^{\pi\lambda\,h^2\left(\frac{-\,(s\,A)^{\frac{2}{\alpha}}}{h^2}\,\Gamma\left(1-\frac{2}{\alpha}\right)+1\right)}, & \left|\frac{s\,A}{h^\alpha}\right| > c. \end{cases}$$

No analytical solution exists for c, the intersection point of the two parts of the absolute value of this function. There is a finite number of solutions. For numerical calculations, it is preferable to take the largest solution in absolute value.

Theorem 9. *Let $A = p \cdot B$ where $p = \frac{EIRP}{4\pi}$ and $B \sim Exp(1)$, an exponential random variable with unit rate, so that $\mathbb{E}[B] = 1$. The Laplace transform of the total power density for the Rayleigh-fading case is then*

$$\mathcal{L}^{Ray.}_{S_{WN}}(s) = \exp\left(\frac{-2\pi\lambda}{\alpha-2}\,sph^{2-\alpha}\,{}_2F_1\left(1, 1-\frac{2}{\alpha}; 2-\frac{2}{\alpha}; \frac{-s\,p}{h^\alpha}\right)\right).$$

Proof. For a Rayleigh fading,

$$\mathbb{E}_A\left[\exp\left(-s\,\frac{A}{x}\right)\right] = \frac{1}{1+\frac{p\,s}{x}}.$$

This expression can be replaced in the Laplace transform of Lemma 1. The change of variable $x\,h^{-\alpha}-1 \to y$ then leads to

$$\mathcal{L}^{Ray.}_{S_{WN}}(s) = \exp\left(\frac{-2\pi\lambda}{\alpha}\,sph^{2-\alpha}\int_0^\infty \frac{1}{y+s\,p\,h^{-\alpha}+1}\,(y+1)^{\frac{2}{\alpha}-1}\,\mathrm{d}y\right)$$

Finally, the expression of Theorem 9 is obtained using the relationship [31]

$$\int_0^\infty t^{-b+c-1}\,(t+1)^{a-c}\,(t-z+1)^{-a}\,\mathrm{d}t = \frac{\Gamma(b)\,\Gamma(c-b)}{\Gamma(c)}\,{}_2F_1(a,b;c;z)$$

where ${}_2F_1(a,b;c;z)$ is the Gauss confluent hypergeometric function. □

The CDF of S_{WN} is then obtained numerically by applying the inversion theorem [32] that we recall in the following theorem.

Theorem 10. *If S is a one-dimensional distribution function, its CDF is given by the following expression for which t is real:*

$$F(x) = \frac{1}{2} - \frac{1}{\pi}\int_0^\infty \frac{\Im\left[\mathrm{e}^{-itx}\,\mathcal{L}_S(-it)\right]}{t}\,dt.$$

Consequently, using the relationship $E = \sqrt{Z_0 \cdot S}$ for the x-axis, we finally obtain the CDF of E. A comparison between CDFs with and without unit-rate Rayleigh-fading is shown in Fig. 3. As expected, probabilities of exceeding any electric field strength is lower in the Rayleigh-fading case. The difference with the no-fading case is however small, as suggests the Kolmogorov-Smirnov distance of 0.07 between the CDFs. In the following, we only work under a no-fading hypothesis. To recall, the aim of this paper is to introduce a simple and quick method for assessing exposure, which can then be used to accurately study the impact of an increase in base station density, for example. The numerical calculation of the Laplace transform of S_{WN} being several orders of magnitude faster under the assumption of no-fading, thanks to the approximation given by Proposition 2, we will only work under this hypothesis in the following. The fitting method proposed in the next section would have been exactly the same if we had not worked under this assumption. Exposure being slightly larger without considering fading, the hypothesis is also consistent with the conservative approach

This article has been accepted for publication in a future issue of this journal, but has not been fully edited. Content may change prior to final publication. Citation information: DOI 10.1109/ACCESS.2021.3091804, IEEE Access

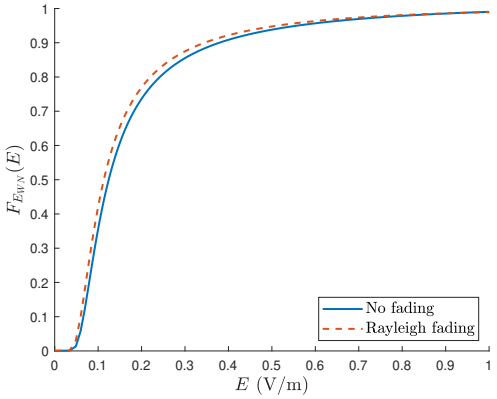

FIGURE 3. CDF $F_{E_{WN}}$ with a Rayleigh fading and without fading. $\lambda = 6\,\mathrm{BS/km^2}$, $\alpha = 3.25$, $h = 38\,\mathrm{m}$, EIRP = 67.96 dBm.

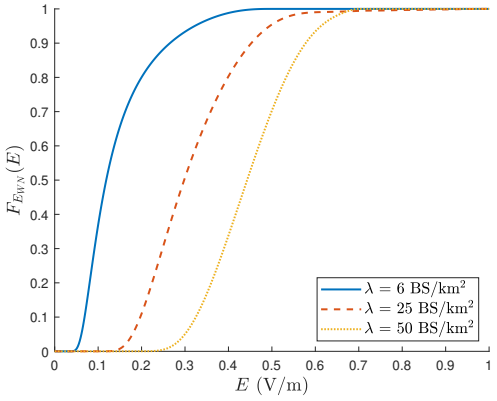

FIGURE 4. CDF $F_{E_{WN}}$ for several values of λ. $\alpha = 3.25$, $h = 38\,\mathrm{m}$, EIRP = 67.96 dBm.

policy advocated by organizations issuing guidelines to limit exposure to EMF. The CDF, for different values of λ, α and h, are respectively shown in Fig. 4, Fig. 5 and Fig. 6, making it possible to observe the impact of these parameters on the shape of the CDF. Clearly, the path loss exponent has the greatest impact on exposure.

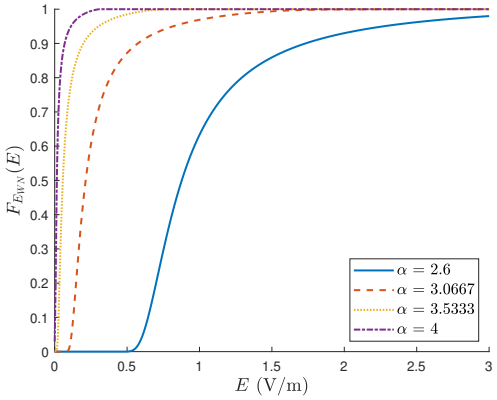

FIGURE 5. CDF $F_{E_{WN}}$ for several values of α. $\lambda = 6\,\mathrm{BS/km^2}$, $h = 38\,\mathrm{m}$, EIRP = 67.96 dBm.

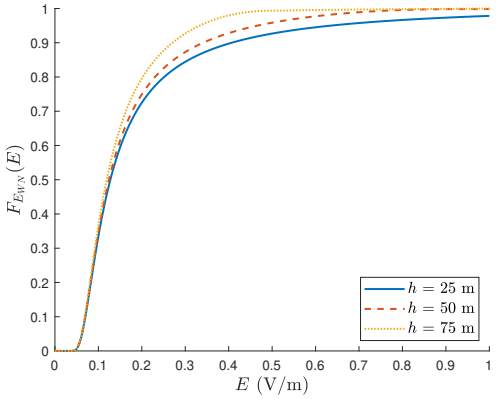

FIGURE 6. CDF $F_{E_{WN}}$ for several values of h. $\lambda = 6\,\mathrm{BS/km^2}$, $\alpha = 3.25$, EIRP = 67.96 dBm.

III. EXPERIMENTAL RESULTS

Using the Brussels database of BS locations, the BS density for each frequency band was calculated over a $4.5\,\mathrm{km^2}$-area that is spread over two municipalities of Brussels, Belgium. All network providers and all communication standards were combined since we cannot differentiate by measurements the technology used in a frequency band. The BS density is $16\,\mathrm{BS/km^2}$ and $6\,\mathrm{BS/km^2}$ for the 2100 MHz and 2600 MHz bands, respectively.

Statistical distributions for the power density were experimentally obtained by drive-tests in this Brussels area. The comprehensive experimental set-up is described in [2]. A spectrum analyzer was mounted on a moving car, taking calibrated measurements along the three polarization axes in the 2100 MHz and 2600 MHz frequency bands with a resolution bandwith of 3 MHz. A GPS was used to tag the measurements with position. Measurements were averaged over squared local areas of $2\,\mathrm{m} \times 2\,\mathrm{m}$. This size was chosen heuristically, small enough to keep the spatial sampling relevant, but large enough to smooth out fading. Measurements were obtained for around 16 000 $4\,\mathrm{m^2}$-squares. We focused on the UMTS 2100, LTE 2100 and LTE 2600 bands:

$$S_{2100} = \sum_{f=2\,110.3\,\mathrm{MHz}}^{2\,140.1\,\mathrm{MHz}} S_f + \sum_{f=2\,154.9\,\mathrm{MHz}}^{2\,169.7\,\mathrm{MHz}} S_f \tag{11}$$

$$S_{2600} = \sum_{f=2\,620\,\mathrm{MHz}}^{2\,640\,\mathrm{MHz}} S_f + \sum_{f=2\,655\,\mathrm{MHz}}^{2\,690\,\mathrm{MHz}} S_f \tag{12}$$

where S_f is the power density measured at frequency f.

Parameters of the model (1)-(3) under the no-fading hypothesis have first been fitted by minimizing

$$\begin{aligned} K(\theta) = &\left(\frac{Q_{05}(\theta)}{Q_{05,exp}} - 1\right)^2 + \left(\frac{Q_{10}(\theta)}{Q_{10,exp}} - 1\right)^2 + \left(\frac{Q_{25}(\theta)}{Q_{25,exp}} - 1\right)^2 \\ &+ \left(\frac{Q_{50}(\theta)}{Q_{50,exp}} - 1\right)^2 + \left(\frac{Q_{75}(\theta)}{Q_{75,exp}} - 1\right)^2 + \left(\frac{Q_{90}(\theta)}{Q_{90,exp}} - 1\right)^2 \\ &+ \left(\frac{Q_{95}(\theta)}{Q_{95,exp}} - 1\right)^2 + \left(\frac{\mu(\theta)}{\mu_{exp}} - 1\right)^2 \end{aligned} \tag{13}$$

This article has been accepted for publication in a future issue of this journal, but has not been fully edited. Content may change prior to final publication. Citation information: DOI 10.1109/ACCESS.2021.3091804, IEEE Access

where $\theta = (h, \alpha, \text{EIRP})$ is the 3-tuple of parameters. Q_x is the x%-quantile and μ the mean of the distribution of S_{WN} using θ. The notation "x_{exp}" refers to statistics obtained from the experimental distribution. The minimization of $K(\theta)$ is an exhaustive search onto a regular grid $\mathcal{G} = \mathcal{I}_h \times \mathcal{I}_\alpha \times \mathcal{I}_{\text{EIRP}}$ with $\mathcal{I}_h = [10; 60]$m with a step of 1 m, $\mathcal{I}_\alpha = [2; 5]$ with a step of 0.05 and $\mathcal{I}_{\text{EIRP}} = [56.0; 81.0]$dBm with a step of 0.01 dBm. In a second phase, the median of the distributions of heights and EIRPs, computed thanks to Brussels database, were taken as values of h and EIRP in the model. The model was then calibrated by minimizing $K(\theta)$ with the remaining unknown parameter $\theta = \alpha$.

Statistical parameters of the distributions are listed in Tables 1 and 2 for the 2100 MHz and 2600 MHz frequency bands, respectively. The optimal sets of parameters θ for the propagation model (3) are also listed in this table. Fixed parameters, estimated a priori from the existing databases, are marked with a star * for clarity.

TABLE 1. *Parameters of the statistical distributions of the power density for the 2100 MHz frequency band, in the Brussels-Capital Region (Ixelles and Etterbeek). Exp: experimental results. SG: CDF obtained by a numerical Gil-Pelaez inversion. Q_x's are the quantiles, μ the mean.*

Frequency band	UMTS 2100 + LTE 2100		
	Exp	SG - $\theta = (h, \alpha, \text{EIRP})$	SG - $\theta = (\alpha)$
λ (BS/km^2)		16.66^*	16.66^*
h (m)		32	28^*
α		3.55	3.45
EIRP (dBm)		67.76	65.45^*
Q_{05} (W/m^2)	$5.38 \cdot 10^{-06}$	$6.91 \cdot 10^{-06}$	$7.54 \cdot 10^{-06}$
Q_{10} (W/m^2)	$7.59 \cdot 10^{-06}$	$9.42 \cdot 10^{-06}$	$1.01 \cdot 10^{-05}$
Q_{25} (W/m^2)	$1.64 \cdot 10^{-05}$	$1.70 \cdot 10^{-05}$	$1.76 \cdot 10^{-05}$
Q_{50} (W/m^2)	$4.25 \cdot 10^{-05}$	$3.83 \cdot 10^{-05}$	$3.90 \cdot 10^{-05}$
Q_{75} (W/m^2)	$1.33 \cdot 10^{-04}$	$1.17 \cdot 10^{-04}$	$1.16 \cdot 10^{-04}$
Q_{90} (W/m^2)	$3.67 \cdot 10^{-04}$	$3.91 \cdot 10^{-04}$	$4.02 \cdot 10^{-04}$
Q_{95} (W/m^2)	$6.57 \cdot 10^{-04}$	$7.85 \cdot 10^{-04}$	$8.60 \cdot 10^{-04}$
μ (W/m^2)	$1.64 \cdot 10^{-04}$	$1.49 \cdot 10^{-04}$	$1.68 \cdot 10^{-04}$
KS distance		0.04	0.06

TABLE 2. *Parameters of the statistical distributions of the power density for the 2600 MHz frequency band, in the Brussels-Capital Region (Ixelles and Etterbeek). Exp: experimental results. SG: CDF obtained by a numerical Gil-Pelaez inversion. Q_x's are the quantiles, μ the mean.*

Frequency band	LTE 2600		
	Exp	SG - $\theta = (h, \alpha, \text{EIRP})$	SG - $\theta = (\alpha)$
λ (BS/km^2)		6.48^*	6.48^*
h (m)		38	33^*
α		3.25	3.20
EIRP (dBm)		67.96	65.75^*
Q_{05} (W/m^2)	$1.08 \cdot 10^{-05}$	$1.01 \cdot 10^{-05}$	$1.07 \cdot 10^{-05}$
Q_{10} (W/m^2)	$1.17 \cdot 10^{-05}$	$1.32 \cdot 10^{-05}$	$1.32 \cdot 10^{-05}$
Q_{25} (W/m^2)	$1.64 \cdot 10^{-05}$	$2.07 \cdot 10^{-05}$	$2.07 \cdot 10^{-05}$
Q_{50} (W/m^2)	$3.91 \cdot 10^{-05}$	$4.21 \cdot 10^{-05}$	$4.02 \cdot 10^{-05}$
Q_{75} (W/m^2)	$1.30 \cdot 10^{-04}$	$1.16 \cdot 10^{-04}$	$1.07 \cdot 10^{-04}$
Q_{90} (W/m^2)	$3.72 \cdot 10^{-04}$	$3.83 \cdot 10^{-04}$	$3.55 \cdot 10^{-04}$
Q_{95} (W/m^2)	$6.64 \cdot 10^{-04}$	$8.29 \cdot 10^{-04}$	$7.94 \cdot 10^{-04}$
μ (W/m^2)	$1.80 \cdot 10^{-04}$	$1.72 \cdot 10^{-04}$	$1.73 \cdot 10^{-04}$
KS distance		0.07	0.08

As seen in Fig. 7 and Fig. 8, the SG CDFs well fit the experimental ones. The x-axis is expressed in terms of electric field strength E instead of power density using (1). To estimate goodness-of-fit, the two-sample Kolmogorov-Smirnov (KS) distance, based on cumulative distribution functions,

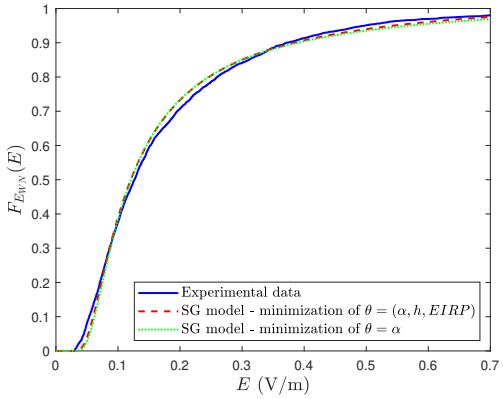

FIGURE 7. CDF of E for the network made of BSs from all network providers in Brussels for the 2100 MHz band.

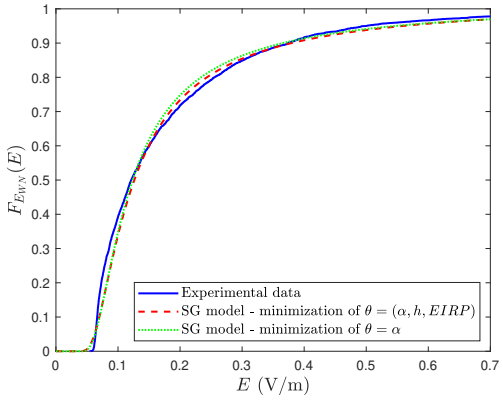

FIGURE 8. CDF of E for the network made of BSs from all network providers in Brussels for the 2600 MHz band.

is computed at the end of the table. The error between the experimental and simulated distributions is of the order of magnitude of the accuracy of the measuring device. Fitted values for optimal parameters $\theta = (h, \alpha, \text{EIRP})$ are realistic on physical grounds. Indeed, values obtained for h and EIRP are very close to the medians of the database distributions. Values of α for the two calibrations $\theta = (h, \alpha, \text{EIRP})$ and $\theta = \alpha$ are close whether or not the height and EIRP are fixed. Parameter α is very close to path loss exponents from deterministic models of the literature, computed in urban environments similar to Brussels. For example, Ichitsubo et al. [8] obtained $\alpha = 3.1$ for a center frequency of 2600 MHz and the COST231 model [7] gives $\alpha = 3.55$ for a BS height of 27 m up to 2 GHz, very close to 2100 MHz.

Two approaches can then be followed to estimate the model parameters. The first approach requires pre-calibration with experimental data through the minimization of $K(\theta)$ in the city of interest. If experimental data is not available, the height, density and EIRP can be deduced from an antenna database while the path loss exponent can be retrieved from a similar path loss model in the literature, at the price of a less good fitting to experimental CDFs. Note that the model parameters must be determined once and for all: they can

This article has been accepted for publication in a future issue of this journal, but has not been fully edited. Content may change prior to final publication. Citation information: DOI 10.1109/ACCESS.2021.3091804, IEEE Access

then be used as a basis for studies such as BS densification, for example.

Taking the distribution of the power density due to the nearest BS, S_1, leads to a mean power density of $1.39 \cdot 10^{-4}\,\mathrm{W/m^2}$ (computed from Corollary 1) instead of $1.72 \cdot 10^{-4}\,\mathrm{W/m^2}$ when considering all BSs (from Theorem 6) for the LTE 2600 frequency band with optimized h, α and EIRP parameters. Expressed in terms of the electric field strengths, these values respectively correspond to $0.23\,\mathrm{V/m}$ and $0.25\,\mathrm{V/m}$. Similarly, for the LTE 2600 band, the 50%- and 95%-quantiles of the electric field are respectively $0.08\,\mathrm{V/m}$ and $1.51\,\mathrm{V/m}$ for the nearest-BS approximation against $0.13\,\mathrm{V/m}$ and $0.56\,\mathrm{V/m}$ when the whole set of BSs is considered.

IV. CONCLUSION

In this paper, we have introduced the use of stochastic geometry for exposure assessment. We have shown some general mathematical expressions of the statistics of the power density, coming from a limited number of the network's BSs or from all BSs. In particular, we have obtained a numerical CDF of the power density due to all BSs for a simple propagation model, when the BS pattern can be approached by a PPP. We have then applied this framework to experimental measurements realized in Brussels, Belgium. We have shown that the model faithfully reproduces real-world values at 2.1 GHz and 2.6 GHz, bands for which the base station densities are very different. As this model only differs for the different frequency bands in its parameters, i.e. density, height, EIRP and path loss exponent, the model is generic and can be applied to any 5G-like frequencies. However, the validation would require measurements performed at these frequencies.

.

APPENDIX A PROOF OF THEOREM 5

The k^{th} moment of the resulting power density from the n nearest BSs is given by

$$\begin{aligned}\mathbb{E}\left[S_{[n]}^k\right] &= \mathbb{E}\left[\left(\sum_{i=1}^{n} S(r_i)\right)^k\right] \\ &= \sum_{k_1+k_2+\ldots+k_n=k} \binom{k}{k_1, k_2, \cdots, k_n} \mathbb{E}\left[S_1^{k_1} S_2^{k_2} \cdots S_n^{k_n}\right] \\ &= \sum_{|\vec{k}|=k} \binom{k}{\vec{k}} \mathbb{E}\left[\prod_{i=1}^{n} S_i^{k_i}\right]\end{aligned} \tag{14}$$

using the multinomial theorem [33], where

$$\binom{n}{k_1, k_2, k_3, \ldots, k_m} = \binom{n}{\vec{k}} = \frac{n!}{k_1! k_2! k_3! \cdots k_m!} = \frac{n!}{\prod_{i=1}^{m} k_i!} \tag{15}$$

is a multinomial coefficient, generalization of the binomial coefficients. To evaluate the quantity

$$\mathbb{E}\left[S_1^{m_1} S_2^{m_2} S_3^{m_3} \cdots S_n^{m_n}\right], \tag{16}$$

we need to first introduce some notations and properties. In the following, we define $M = \sum_{i=1}^{n} m_i$ and we use the properties

$$\tau_i = \tau_{(i)}^{(i)}, \tag{17}$$

$$\tau_{(a)}^{(b)} + \tau_{(b+1)}^{(c)} = \tau_{(a)}^{(c)}, \tag{18}$$

for which the notation $\tau_{(a)}^{(b)}$ has been defined in the statement of Theorem 5.

Moreover, we use, as previously, the change of variable $\lambda\pi\left(r_i^2 + h^2\right) \to t_i$ and the following lemmas involving the upper incomplete Gamma function:

Lemma 2. *The integration property of the incomplete Gamma function is*

$$\int_l^\infty t^{b-1}\,\Gamma(z,t)\,\mathrm{d}t = \frac{1}{b}\left(\Gamma(b+z,l) - l^b\,\Gamma(z,l)\right).$$

Proof. The proof is immediate using an integration by parts and the result $\lim_{t\to\infty} t^b\,\Gamma(z,t) = 0$. □

Lemma 3. *In the particular case $b = 1$, Lemma 2 has a simplified statement*

$$\int_l^\infty \Gamma(z,t)\,\mathrm{d}t = \Gamma(1+z,l) - l\,\Gamma(z,l).$$

Lemma 4. *The recurrence formula of the incomplete Gamma function is*

$$\Gamma(z+1,t) = t^z\,\mathrm{e}^{-t} + z\,\Gamma(z,t).$$

Proof. Using the definition of the incomplete Gamma function twice and using an integration by parts, we obtain

$$\begin{aligned}\Gamma(z+1,t) &= \int_t^\infty u^z\,\mathrm{e}^{-u}\,\mathrm{d}u \\ &= \left[-u^z\,\mathrm{e}^{-u}\right]_t^\infty + z\int_t^\infty u^{z-1}\,\mathrm{e}^{-u}\,\mathrm{d}u \\ &= t^z\,\mathrm{e}^{-t} + z\,\Gamma(z,t).\end{aligned}$$

□

Using the joint probability distribution for the n nearest BSs

$$\begin{aligned}&f(r_1, r_2, \cdots, r_n)\,\mathrm{d}r_1\,\mathrm{d}r_2\cdots\mathrm{d}r_n \\ &\qquad = (2\lambda\pi)^n\,\mathrm{e}^{-\lambda\pi r_n^2}\,r_1\,r_2\cdots r_n\,\mathrm{d}r_1\,\mathrm{d}r_2\cdots\mathrm{d}r_n,\end{aligned} \tag{19}$$

the quantity (16) can be expressed as

$$\begin{aligned}\mathbb{E}\left[S_1^{m_1} S_2^{m_2}\cdots S_n^{m_n}\right] &= \overline{A^M}\,(\lambda\pi)^{M\alpha/2}\,\mathrm{e}^{\lambda\pi h^2}\int_{\lambda\pi h^2}^\infty t_1^{-\alpha/2\,m_1} \\ &\times \underbrace{\int_{t_1}^\infty t_2^{-\alpha/2\,m_2}\cdots\int_{t_{n-1}}^\infty t_n^{-\alpha/2\,m_n}\,\mathrm{e}^{-t_n}\,\mathrm{d}t_n\cdots\mathrm{d}t_2}_{*}\,\mathrm{d}t_1.\end{aligned} \tag{20}$$

Let us extract the term underbraced by a star for convenience.

$$
\begin{aligned}
&\int_{t_1}^{\infty} t_2^{-\alpha/2\, m_2} \cdots \int_{t_{n-1}}^{\infty} t_n^{-\alpha/2\, m_n}\, \mathrm{e}^{-t_n}\, \mathrm{d}t_n \cdots \mathrm{d}t_2 \\
&= \int_{t_1}^{\infty} t_2^{-\alpha/2\, m_2} \cdots \int_{t_{n-2}}^{\infty} \Gamma\left(\overbrace{1-\alpha/2\, m_n}^{\tau_n}, t_{n-1}\right) \\
&\quad \times t_{n-1}^{\alpha/2\, m_{n-1}}\, \mathrm{d}t_{n-1} \cdots \mathrm{d}t_2 \\
&= \int_{t_1}^{\infty} t_2^{\tau_2-1} \cdots \int_{t_{n-3}}^{\infty} \frac{1}{\tau_{n-1}} \Big[\Gamma\left(\tau_{(n-1)}^{(n)}, t_{n-2}\right) \\
&\quad - t_{n-2}^{\tau_{n-1}} \Gamma\left(\tau_n, t_{n-2}\right)\Big]\, t_{n-2}^{\tau_{n-2}-1}\, \mathrm{d}t_{n-2} \cdots \mathrm{d}t_2 \\
&= \int_{t_1}^{\infty} t_2^{\tau_2-1} \cdots \int_{t_{n-4}}^{\infty} \Bigg[\frac{1}{\tau_{n-1}\, \tau_{n-2}} \Gamma\left(\tau_{(n-2)}^{(n)}, t_{n-3}\right) \\
&\quad - \frac{t_{n-3}^{\tau_{n-2}}}{\tau_{n-1}\, \tau_{n-2}} \Gamma\left(\tau_{(n-1)}^{(n)}, t_{n-3}\right) - \frac{1}{\tau_{n-1}\, \tau_{(n-2)}^{(n-1)}} \Gamma\left(\tau_{(n-2)}^{(n)}, t_{n-3}\right) \\
&\quad + \frac{t_{n-3}^{\tau_{(n-2)}^{(n-1)}}}{\tau_{n-1}\, \tau_{(n-2)}^{(n-1)}} \Gamma\left(\tau_n, t_{n-3}\right)\Bigg]\, t_{n-3}^{\tau_{n-3}-1}\, \mathrm{d}t_{n-3} \cdots \mathrm{d}t_2 \\
&= \int_{t_1}^{\infty} t_2^{\tau_2-1} \cdots \int_{t_{n-4}}^{\infty} \Bigg[\frac{1}{\tau_{(n-2)}^{(n-1)}\, \tau_{(n-2)}^{(n-2)}} \Gamma\left(\tau_{(n-2)}^{(n)}, t_{n-3}\right) \\
&\quad - \frac{t_{n-3}^{\tau_{(n-2)}^{(n-2)}}}{\tau_{(n-1)}^{(n-1)}\, \tau_{(n-2)}^{(n-2)}} \Gamma\left(\tau_{(n-1)}^{(n)}, t_{n-3}\right) \\
&\quad + \frac{t_{n-3}^{\tau_{(n-2)}^{(n-1)}}}{\tau_{(n-1)}^{(n-1)}\, \tau_{(n-2)}^{(n-1)}} \Gamma\left(\tau_{(n)}^{(n)}, t_{n-3}\right)\Bigg]\, t_{n-3}^{\tau_{n-3}-1}\, \mathrm{d}t_{n-3} \cdots \mathrm{d}t_2 \\
&= \ldots \\
&= \sum_{p=1}^{n-1} (-1)^{p-1} \left(\prod_{j=p+1}^{n-1} \frac{1}{\tau_{(p+1)}^{(j)}}\right) \left(\prod_{l=2}^{p} \frac{1}{\tau_{(l)}^{(p)}}\right) \Gamma\left(\tau_{(p+1)}^{(n)}, t_1\right)\, t_1^{\tau_{(2)}^{(p)}}
\end{aligned}
\tag{21}
$$

Using (18) and replacing (21) in (20), we obtain the theorem:

$$
\begin{aligned}
\mathbb{E}\left[S_1^{m_1} S_2^{m_2} \cdots S_n^{m_n}\right] &= \overline{A^M}\, (\lambda\pi)^{M\alpha/2}\, \mathrm{e}^{\lambda\pi h^2} \sum_{p=1}^{n-1} (-1)^{p-1} \\
&\times \left(\prod_{j=p+1}^{n-1} \frac{1}{\tau_{(p+1)}^{(j)}}\right) \left(\prod_{l=1}^{p} \frac{1}{\tau_{(l)}^{(p)}}\right) \left[\tilde{\Gamma}_{\tau_{(1)}^{(n)}} - \left(\lambda\pi h^2\right)^{\tau_{(1)}^{(p)}}\, \tilde{\Gamma}_{\tau_{(p+1)}^{(n)}}\right].
\end{aligned}
\tag{22}
$$

REFERENCES

[1] S. Aerts, L. Verloock, M. Van Den Bossche, D. Colombi, L. Martens, C. Törnevik, and W. Joseph, "In-situ Measurement Methodology for the Assessment of 5G NR Massive MIMO Base Station Exposure at Sub-6 GHz Frequencies," IEEE Access, vol. 7, pp. 184658–184667, 2019.

[2] T. Lemaire, J. Wiart, and P. De Doncker, "Variographic analysis of public exposure to electromagnetic radiation due to cellular base stations: Variographic Analysis of BTS EMF Exposure," Bioelectromagnetics, vol. 37, 10 2016.

[3] M. Cansiz, T. Abbasov, M. B. Kurt, and A. R. Celik, "Mobile measurement of radiofrequency electromagnetic field exposure level and statistical analysis," Measurement, vol. 86, pp. 159–164, 2016.

[4] S. Aerts, J. Wiart, L. Martens, and W. Joseph, "Assessment of long-term spatio-temporal radiofrequency electromagnetic field exposure," Environmental Research, vol. 161, pp. 136 – 143, 2018.

[5] M. Celaya-Echarri, L. Azpilicueta, J. Karpowicz, V. Ramos, P. Lopez-Iturri, and F. Falcone, "From 2G to 5G Spatial Modeling of Personal RF-EMF Exposure Within Urban Public Trams," IEEE Access, vol. 8, pp. 100930–100947, 2020.

[6] S. Shikhantsov, A. Thielens, G. Vermeeren, P. Demeester, L. Martens, G. Torfs, and W. Joseph, "Massive MIMO Propagation Modeling With User-Induced Coupling Effects Using Ray-Tracing and FDTD," IEEE Journal on Selected Areas in Communications, vol. 38, no. 9, pp. 1955–1963, 2020.

[7] E. Damasso and L. Correia, "COST Action 231: Digital Mobile Radio Towards Future Generation Systems: Final Report," tech. rep., European Commission, 1999.

[8] S. Ichitsubo, T. Furuno, T. Taga, and R. Kawasaki, "Multipath propagation model for line-of-sight street microcells in urban area," IEEE Transactions on Vehicular Technology, vol. 49, no. 2, pp. 422–427, 2000.

[9] P. Kyösti, J. Meinilä, L. Hentila, X. Zhao, T. Jämsä, C. Schneider, M. Narandzic, M. Milojević, A. Hong, J. Ylitalo, V.-M. Holappa, M. Alatossava, R. Bultitude, Y. Jong, and T. Rautiainen, "WINNER II channel models," IST-4-027756 WINNER II D1.1.2 V1.2, 02 2008.

[10] B. Thors, A. Furuskär, D. Colombi, and C. Törnevik, "Time-Averaged Realistic Maximum Power Levels for the Assessment of Radio Frequency Exposure for 5G Radio Base Stations Using Massive MIMO," IEEE Access, vol. 5, pp. 19711–19719, 2017.

[11] E. Chiaramello, D. Plets, S. Fiocchi, M. Bonato, G. Tognola, M. Parazzini, L. Le Brusquet, W. Joseph, and P. Ravazzani, "Innovative stochastic modeling of residential exposure due to a WiFi source placed in uncertain position," in BioEM2019 - Annual Joint Meeting of the Bioelectromagnetics Society (BEMS) and the European BioElectromagnetics Association (EBEA), (Montpellier, France), June 2019.

[12] F. Baccelli and B. Blaszczyszyn, "Stochastic Geometry and Wireless Networks: Volume I Theory," Foundations and Trends in Networking, vol. 3, pp. 249–449, 01 2009.

[13] A. Al-Hourani, R. J. Evans, S. Kandeepan, B. Moran, and H. Eltom, "Stochastic Geometry Methods for Modeling Automotive Radar Interference," IEEE Transactions on Intelligent Transportation Systems, vol. 19, no. 2, pp. 333–344, 2018.

[14] C. E. O'Lone, H. S. Dhillon, and R. M. Buehrer, "A Statistical Characterization of Localization Performance in Wireless Networks," IEEE Transactions on Wireless Communications, vol. 17, no. 9, pp. 5841–5856, 2018.

[15] M. Filo, C. H. Foh, S. Vahid, and R. Tafazolli, "Stochastic Geometry Analysis of Ultra-Dense Networks: Impact of Antenna Height and Performance Limits," 2017.

[16] R. Mathar and J. Mattfeldt, "On the distribution of cumulated interference power in Rayleigh fading channels," Wireless Networks, vol. 1, no. 1, pp. 31–36, 1995.

[17] J. Andrews, A. Gupta, and H. Dhillon, "A Primer on Cellular Network Analysis Using Stochastic Geometry," 04 2016.

[18] M. A. Hajj, S. Wang, P. De Doncker, C. Oestges, and J. Wiart, "A Statistical Estimation of 5G Massive MIMO's Exposure using Stochastic Geometry," in 2020 XXXIIIrd General Assembly and Scientific Symposium of the International Union of Radio Science, pp. 1–3, 2020.

[19] ICNIRP, "ICNIRP Guidelines for Limiting Exposure to Electromagnetic Fields (100 kHz to 300 GHz)," Health Physics, vol. 118, pp. 483–524, 2020.

[20] I. T. Union, "Measurement of radio frequency electromagnetic fields to determine compliance with human exposure limits when a base station is put into service," 2019. 07/2019. FEMU ID: 39880; EMF-Portal URL: https://www.emf-portal.org/en/article/39880.

[21] J. S. Gomez, A. Vasseur, A. Vergne, P. Martins, L. Decreusefond, and W. Chen, "A Case Study on Regularity in Cellular Network Deployment," IEEE Wireless Communications Letters, vol. 4, pp. 421–424, Aug 2015.

[22] J. F. C. Kingman, Poisson processes, vol. 3 of Oxford Studies in Probability, ch. Sums over Poisson processes, pp. 28–29. New York: The Clarendon Press Oxford University Press, 1993. Oxford Science Publications.

[23] H. Thompson, "Distribution of distance to nth neighbour in a population of randomly distributed individuals," Ecology, vol. 37, 1956.

[24] M. Abramowitz and I. A. Stegun, Handbook of Mathematical Functions with Formulas, Graphs, and Mathematical Tables, ch. Gamma Function and Related Function, p. 263. New York: Dover, 9th Dover printing, 10th GPO printing ed., 1964.

[25] W. Bi, L. Xiao, X. Su, and S. Zhou, "Fractional full duplex cellular network: a stochastic geometry approach," Science China Information Sciences, vol. 61, pp. 1–15, 2016.

[26] F. Baccelli and B. Błaszczyszyn, "Stochastic Geometry and Wireless Networks: Volume II Applications," Foundations and Trends in Networking, vol. 4, no. 1–2, pp. 1–312, 2010.

[27] A. Aravanis, T. Tu, O. Muñoz, A. Pascual-Iserte, and M. Di Renzo, "A tractable closed form approximation of the ergodic rate in Poisson cellular networks," EURASIP Journal on Wireless Communications and Networking, vol. 12, 12 2019.

[28] L. T. Tu, New Analytical Methods for the Analysis and Optimization of Energy-Efficient Cellular Networks by Using Stochastic Geometry. Theses, Université Paris-Saclay, June 2018.
[29] M. Haenggi, Stochastic Geometry for Wireless Networks. Cambridge University Press, 2012.
[30] M. Renzo and W. Lu., "System-level analysis/optimization of cellular networks with simulataneous wireless information and power transfer: Stochastic geometry modeling," IEEE Transactions on Vehicular Technology, vol. 66, pp. 2251–2275, 2017.
[31] S. Saran, "Hypergeometric functions of three variables," Ganita, vol. 5, no. 2, pp. 77–91, 1954.
[32] J. Gil-Pelaez, "Note on the inversion theorem," Biometrika, vol. 38, pp. 481–482, 12 1951.
[33] K. K. Kataria, "A Probabilistic Proof of the Multinomial Theorem," The American Mathematical Monthly, vol. 123, no. 1, pp. 94–96, 2016.

QUENTIN GONTIER was born in Brussels in 1997. He received the B.S. and M.S. degrees in physics engineering from the Université Libre de Bruxelles, Belgium, in 2020. Since 2020, he his a Ph.D. student in the Wireless Communications Group at the Université Libre de Bruxelles. His research interests include stochastic geometry and ray-tracing modeling applied to exposure assessment.

LUCAS PETRILLO was born in Genoa, Italy in 1984. He graduated in electronic engineering from the University of Genoa, Italy, in 2008. He received the Master's degree in communication systems and the Doctoral degree from the University Pierre et Marie Curie, Paris, France, in 2008 and 2011, respectively. From 2008 to 2011 he was a researcher at Onera, France. From 2011 to 2012 he was an Assistant Teacher at the University Pierre et Marie Curie, where he taught electronics. From 2012 to 2019 he was a postdoctoral researcher at the Université Libre de Bruxelles, Belgium. Since 2020, he is with Bruxelles Environnement, Belgium, where he is involved in EMF regulations for the Brussels-Capital Region. His scientific interests includes electromagnetics propagation in complex media, communication systems and mapping of EMF exposure.

FRANÇOIS ROTTENBERG (S'15–M'18) received the M.Sc. in Electrical Engineering from the Université catholique de Louvain (UCLouvain), Louvain-la-Neuve, in 2014, and the Ph.D. degree jointly from UCLouvain and Université libre de Bruxelles (ULB), Brussels, in 2018. From September 2018 to August 2019, he was a postdoctoral researcher with the University of Southern California (USC), Los Angeles, U.S.A, leading the 5G massive MIMO research efforts. He is now a postdoctoral researcher affiliated with UCLouvain and ULB, funded by the Belgian National Science Foundation (FRS-FNRS). He participated to various national, European and international projects. From 2015, he has been a regular visitor and collaborator of the Centre Tecnològic Telecomunicacions Catalunya (CTTC), Castelldefels, Spain and National Institute of Information and Communications Technology (NICT), Tokyo, Japan. His main research interests are in signal processing for next generations of communication systems, including novel modulation formats, multi-antenna systems and physical-layer security.

FRANÇOIS HORLIN received the Ph.D. degree from the Université catholique de Louvain (UCL) in 2002. He specialized in the field of signal processing for digital communications. After his Ph.D., he joined the Inter-university Micro-Electronics Center (IMEC). He led the project aiming at developing a 4G cellular communication system in collaboration with Samsung Korea. In 2007, François Horlin became professor at the Université libre de Bruxelles (ULB). He is currently supervising a research team working on next generation communication systems. Localization based on 5G signals, filterbank-based modulations, massive MIMO and dynamic spectrum access are examples of currently investigated research topics. He has been academic representative to the executive board of ULB from 2010 to 2015. Since 2017, he is vice dean for research at the Ecole Polytechnique de Bruxelles (EPB).

JOE WIART , PhD (95), Engineer of Telecommunication (92) is since 2015 the holder of the Chair C2M "Caractérisation, modélisation et maîtrise of the Institut Mines Telecom" (https://chairec2m.wp.imt.fr) at Telecom-Paris. Since 2018 he is the president of "Comité d'orientation de l'observatoire des ondes de la ville de Paris". He is also the Chairman of the TC106x of the European Committee for Electrotechnical Standardization (CENELEC) in charge of EMF exposure standards. He is the present Chairman of the International Union of Radio Science (URSI) commission k and has been the Chairman of the French chapter of URSI. He is emeritus member of The Society of Electrical Engineers (SEE) since 2008 and senior member of Institute of Electrical and Electronics Engineers (IEEE) since 2002. His research interests are experimental, numerical methods, machine learning and statistic applied in electromagnetism and dosimetry. His works gave rise to more than 150 publications in journal papers and more than 200 communications.

This article has been accepted for publication in a future issue of this journal, but has not been fully edited. Content may change prior to final publication. Citation information: DOI 10.1109/ACCESS.2021.3091804, IEEE Access

CLAUDE OESTGES (Fellow, IEEE) received the M.Sc. and Ph.D. degrees in electrical engineering from the Université catholique de Louvain (UCLouvain), Louvain-la-Neuve, Belgium, in 1996 and 2000, respectively. In 2001, he joined the Smart Antennas Research Group (Information Systems Laboratory), Stanford University, Stanford, CA, USA, as a Post-Doctoral Scholar. From 2002 to 2005, he was a Post-Doctoral Fellow of the Belgian Fonds de la Recherche Scientifique (FRS-FNRS) with the Microwave Laboratory, UCLouvain. He is currently a Full Professor with the Electrical Engineering Department, Institute for Information and Communication Technologies, Electronics and Applied Mathematics, UCLouvain. He has authored or coauthored four books and more than 200 journal articles and conference communications. Dr. Oestges was the Chair of the COST Action CA15104 IRACON from 2016 to 2020, and the recipient of the 1999–2000 IET Marconi Premium Award and the IEEE Vehicular Technology Society Neal Shepherd Award in 2004 and 2012, respectively.

PHILIPPE DE DONCKER received the M.Sc. degree in physics engineering and the Ph.D. degree in science engineering from the Université Libre de Bruxelles (ULB), Brussels, Belgium, in 1996 and 2001, respectively. He is currently a Full Professor with ULB, where he also leads the research activities on wireless channel modeling and electromagnetics.